

the filamentary large-scale structure rather than the position of individual galaxies.

More recently, Tejos et al. (2016) studied Ly α and O VI absorption in a single sightline in regions between galaxy clusters. The detected overdensity of narrow and broad Ly α absorbers hints at the presence of filamentary gas connecting the clusters. A different approach was taken by Wakker et al. (2015). Instead of mapping gas along an isolated sightline, they used several sightlines passing through a known galaxy filament. By comparing the relation of Ly α equivalent width with both galaxy and filament impact parameters, Wakker et al. (2015) conclude that Ly α absorbers are best described in the context of large-scale structure, instead of tracing individual galaxy haloes. While there is a relation between strong ($N(\text{H I}) > 10^{15} \text{ cm}^{-2}$) absorbers and the CGM of galaxies, weak Ly α absorbers are more likely to be associated with filaments. This view is also supported by Penton et al. (2002), who find that weak absorbers do not show a correlation between equivalent width and impact parameter to the nearest galaxy, while stronger absorbers do. By comparing the position of their sample of Ly α absorbers relative to galaxies in filaments, they conclude that the absorbers align with the filamentary structure. Evidence for absorbers tracing an extensive, intra-group medium comes from other recent surveys of Stocke et al. (2013) and Keeney et al. (2018).

While the correlation between Ly α equivalent width and galaxy impact parameter seems to indicate that these absorbers *somehow* are associated with galaxies (e.g., by the gravitational potential), studies like Wakker et al. (2015); Tejos et al. (2016) show that at least some of the absorbers are associated with the cosmological large-scale structure. Others studies (Bowen et al. 2002; Wakker & Savage 2009) conclude that their data simply does not yield any definite conclusions on this aspect (see also Penton et al. 2002; Prochaska et al. 2011; Tejos et al. 2014). Therefore, the question of how Ly α absorbers at $z = 0$ are linked to galaxies and the large-scale cosmological structure is not yet resolved. Clearly, additional absorption-line studies that improve the currently limited statistics on the absorber/galaxy connection are desired.

In this paper, we systematically investigate the properties of $z = 0$ Ly α absorbers and their connection to the local galaxy environments and the surrounding large-scale structure. For this, we follow an approach similar to that of Wakker et al. (2015). We combine the information on local galaxy filaments mapped by Courtois et al. (2013) with archival UV absorption line data from the Cosmic Origins Spectrograph (COS) installed on the *Hubble Space Telescope* (HST).

Information on the galaxy sample used in this study is provided in Sect. 2. In Sect. 3, the HST/COS data are described and information on the absorption line measurements are given. Details on the galaxy filaments are presented in Sect. 4. In Sect. 5, we investigate the relation between absorbers and galaxies, whereas in Sect. 6 we focus on the relation between absorbers and filaments. In Sect. 7, we discuss our findings and compare them with previous studies. Finally, we summarise and conclude our study in Sect. 8.

2. Galaxy data

Courtois et al. (2013) used the V8k catalogue of galaxies to map galaxy filaments in the nearby universe. This catalogue is available from the Extragalactic Distance Database¹ (EDD Tully et al. 2009). It is a compilation of different surveys, including John

Huchra’s ‘ZCAT’ and the IRAS Point Source Catalog redshift survey with its extensions to the Galactic plane (Saunders et al. 2000a,b). In total, the catalogue consists of $\sim 30\,000$ galaxies, all with velocities less than 8000 km s^{-1} . It is complete up to $M_B = -16$ for galaxies at 1000 km s^{-1} , while at 8000 km s^{-1} , it contains one in 13 of the $M_B = -16$ galaxies. A radial velocity of 8000 km s^{-1} corresponds to a cosmological distance of $d \sim (114 \text{ km s}^{-1})h_{70}^{-1}$. The distance to the Centaurus Cluster ($v \sim 3000 \text{ km s}^{-1}$) is $\sim 40 \text{ Mpc}$. As described in Sect. 3, the velocity range studied in this work extends up to $v \sim 6700 \text{ km s}^{-1}$, which corresponds to $\lambda \sim 1243 \text{ \AA}$. Note that distance estimates to galaxies within 3000 km s^{-1} in the V8k catalogue are adjusted to match the Virgo-flow model by Shaya et al. (1995). The relatively uniform sky coverage (except for the zone of avoidance, ZOA) of the V8k survey combined with the broad range of galaxy types make it suitable for qualitative work (Courtois et al. 2013).

The distribution of apparent and absolute B -band magnitudes as well as $\log(L/L^*)$ for all galaxies of the V8k catalogue is presented in Fig. 1. As can be seen from this distribution, the V8k catalogue is largely insensitive to dwarf galaxies with luminosities $\log(L/L^*) \leq -0.5$. This needs to be kept in mind for our later discussion of the absorber-galaxy relation in Sects. 5 and 6. We decided to not add supplementary galaxy data from other surveys, because the sky coverage of such a mixed galaxy sample would be quite inhomogeneous, which would introduce an additional bias to the galaxy-absorber statistics.

In Fig. 2, upper panel, we show the sky distribution of the galaxies in the various filaments, such as defined in Courtois et al. (2013). The galaxies in these filaments have radial veloci-

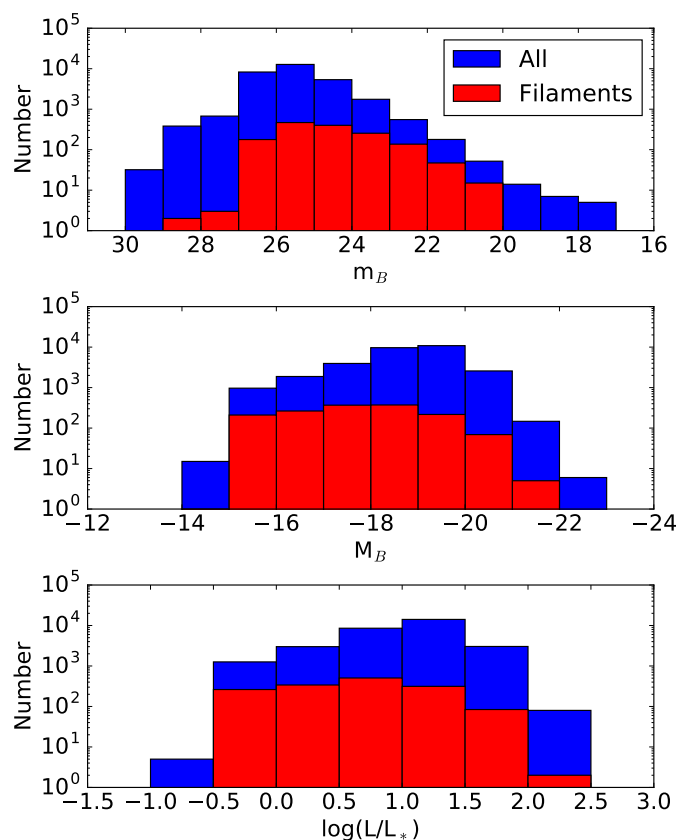


Fig. 1. Histogram of apparent and absolute B -band magnitudes and luminosities for all galaxies of the V8k catalogue.

¹ <http://edd.ifa.hawaii.edu/>

ties in the range $v = 750 - 5900 \text{ km s}^{-1}$. All filaments are feeding into the Centaurus Cluster located at $l \sim 300^\circ$ and $b \sim 20^\circ$. The large concentration of galaxies in the green filament, between $l \sim 260 - 300^\circ$ and $b \sim 60 - 70^\circ$ is due to the Virgo Cluster.

3. Absorption line data

3.1. HST/COS observations

In this study we make use of ancillary HST/COS data, as retrieved from the HST Science Archive at the Canadian Astronomy Data Centre (CADC). The total sample consists of 302 AGN sightlines, all reduced following the procedures described in Richter et al. (2017).

Since the Ly α absorption ($\lambda_0 = 1215.67 \text{ \AA}$) in the spectra studied here falls in the wavelength range between 1215 and 1243 \AA , we make use of the data from the COS G130M grating. This grating covers a wavelength range from 1150 – 1450 \AA and has a resolving power of $R = 16,000 - 21,000$ (Green et al. 2012; Dashtamirova et al. 2018). The data quality in our COS sample is quite diverse, with signal-to-noise (S/N) ratios per resolution element varying substantially (between 3 and 130; see Fig. A.1 in the Appendix.)

We also checked for metal absorption in the Ly α absorbers, considering the transitions of Si III $\lambda 1206.50$, Si II doublet $\lambda 1190.42; 1193.29$, Si II $\lambda 1260.42$, Si II $\lambda 1526.71$, Si IV doublet $\lambda 1393.76; 1402.77$, C II $\lambda 1334.53$, C IV doublet $\lambda 1548.20; 1550.77$. For the lines at $\lambda > 1450 \text{ \AA}$, data from the COS G160M grating was used, which covers $\lambda = 1405 - 1775 \text{ \AA}$.

The QSO sightlines are plotted on top of the V8k galaxy filaments in the lower panel of Fig. 2. The sky coverage of the sightlines is noticeably better in the upper hemisphere. As can be seen, the majority of the sightlines do not pass through the centres of the filaments, but rather are located at the filament edges.

A reason for sightlines not going directly through filaments could be because of extinction. This holds true especially for dense regions like the Virgo Cluster, where the extinction is high. On the other hand, the Virgo Cluster is a nearby cluster and might be better studied than random regions on the sky. From the COS sightlines shown in the lower panel of Fig. 2, no clear bias can be seen, except for the northern versus southern hemisphere.

3.2. Absorber sample and spectral analysis

For all 302 COS spectra, the wavelength range between 1220 – 1243 \AA was inspected for intervening absorption. This range corresponds to Ly α in the velocity range $v \approx 1070 - 6700 \text{ km s}^{-1}$. At velocities $< 1070 \text{ km s}^{-1}$, Ly α absorption typically is strongly blended with the damped Ly α absorption trough from the foreground Galactic interstellar medium (ISM). To ensure consistency, we do not further consider any absorption feature below 1220 \AA .

Each detected absorption feature at 1220 – 1243 \AA was checked to be Ly α absorption by ruling out Galactic foreground ISM absorption and other, red-shifted lines from intervening absorbers at higher redshift. As for the Galactic ISM absorption, this wavelength range contains only the N V doublet (1238, 1242 \AA) and the weak Mg II doublet (1239, 1240 \AA) as potential contaminants and the regions were flagged accordingly. Potential red-shifted contaminating lines that were ruled out include:

the H I Lyman-series up to Ly δ , Si III (1206.50 \AA), and the two O VI lines at 1037.62 and 1031.93 \AA . Whenever possible, we also used the line-list of intergalactic absorbers from Danforth et al. (2016), which covers a sub-sample of 82 COS spectra. All in all, we identify 587 intervening Ly α absorbers along the 302 COS sightlines in the range $\lambda = 1220 - 1243 \text{ \AA}$.

For the continuum normalisation and the equivalent width measurements of the detected features (via a direct pixel integration) we used the span code (Richter et al. 2011) in the ESO-MIDAS software package, which also provides velocities/redshifts for the absorbers. To derive column densities of H I (and the metal ions) for a sub-sample of the identified Ly α absorbers we used the component-modelling method, as described in Richter et al. (2013). In this method, the various velocity sub-components in an absorber are consistently modelled in all available ions (H I and metals) to obtain column densities (N) and Doppler-parameter (b -values) for each ion in each component. Throughout the paper, we give column densities in units [cm^{-2}] and b -values in units [km s^{-1}]. The modelling code, that is also implemented in ESO-MIDAS, takes into account the wavelength dependent line-spread function of the COS instrument. Wavelengths and oscillator strengths of the analysed ion transitions were taken from the list of Morton (2003).

The total sample of 302 COS sightlines was separated into two sub-samples, one with sightlines passing close to a filament, and the other with sightlines that do not. To account for the occasionally seen large projected widths of the filaments (see, e.g., part of the dark blue filament in Fig. 2) and to be able to map also the outer parts of the filaments, a separation of 5 Mpc to the nearest galaxy belonging to a filament was chosen as dividing distance in this selection process. One sightline (towards 4C–01.61) was categorised as belonging to a filament – although its nearest galaxy distance is as large as 7.9 Mpc – because it passes a filament that is very poorly populated. In total, our selection processes lead to 91 sightlines that are categorised as filament-related, while the remaining 211 sightlines are categorised as sightlines that are unrelated to the filaments studied here. The total redshift pathlength in our COS data set can be estimated as $\Delta z = 0.0189 N$, with N being the number of sightlines. This gives $\Delta z = 1.72$ and 3.99 for the sightline sample belonging to filaments and the one unrelated to filaments, respectively. This will be further discussed in Sect. 7.

Within the for us relevant sub-sample of the filament-related sightlines, 12 spectra were unsuited for measurements for absorption-line measurements due to various different data issues, such as an indeterminable continuum, or heavy blending from various lines. Of the remaining 79 spectra, 9 had no Ly α absorption features detected in the studied wavelength range. This implies a Ly α detection rate of $\sim 90\%$ (we will later further discuss the number density and cross section of Ly α absorbers in this sample). The signal-to-noise ratios for these 79 spectra vary between 5 and 92 per resolution element. In this sub-sample of 79 filament-related sightlines, we identify 215 Ly α absorption systems that are composed of 227 individual components. For these 215 (227) absorbers (components), we have derived H I column densities and b -values via the component-modelling method, as described above.

In the other sightline sample, that we categorise as unrelated to the galaxy filaments, 25 spectra were unsuited for measurements for the same reasons as described above. Of the remaining 186 spectra, only 24 show no Ly α absorption in the range considered above, resulting in a 87% detection rate for Ly α in this sample.

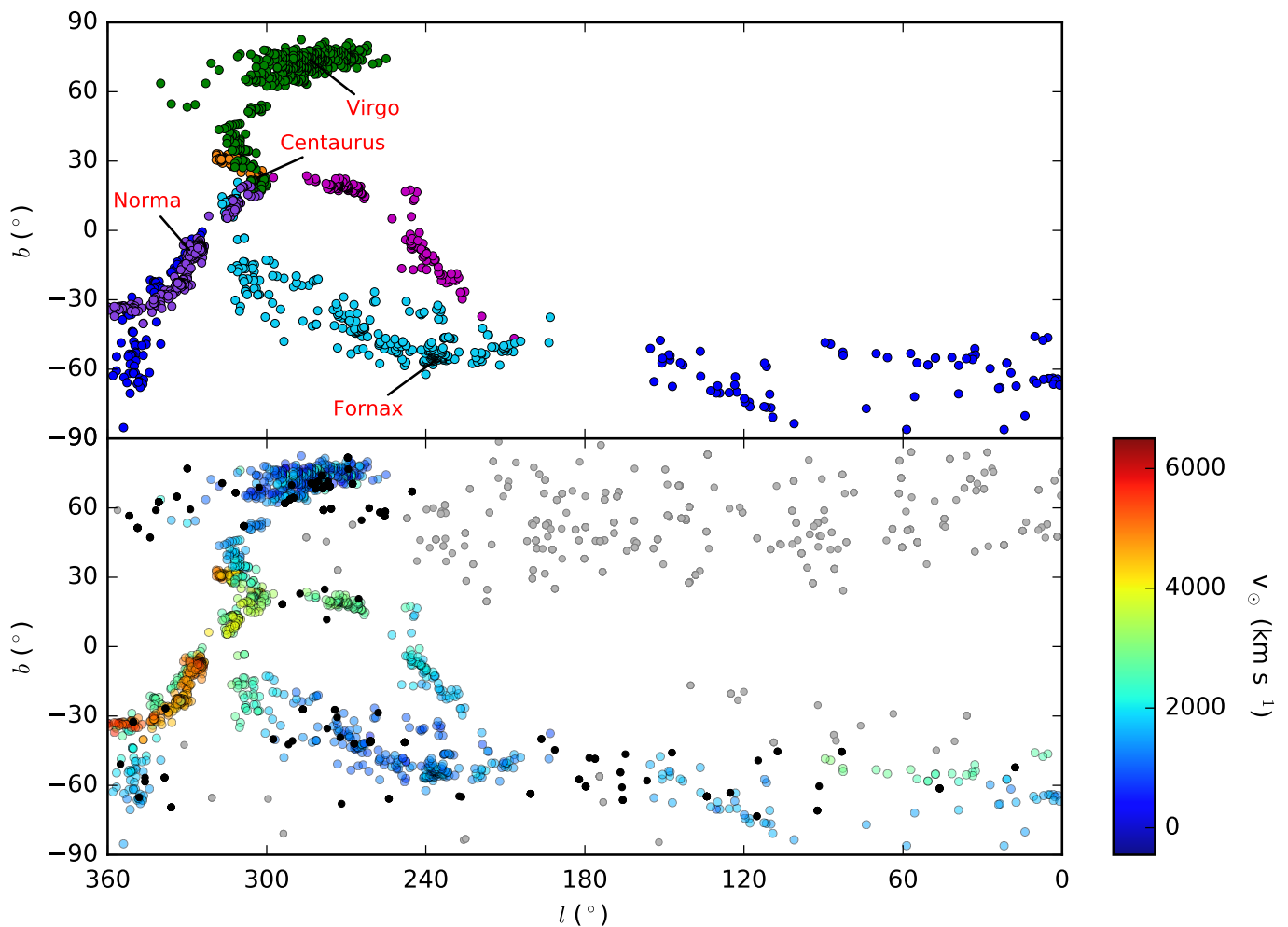


Fig. 2. *Upper panel:* Sky distribution of galaxies from V8k belonging to filaments as defined in Courtois et al. (2013). The different colours indicate different galaxy filaments. Several important clusters are noted. *Lower panel:* Sky distribution of HST/COS sightlines passing close to a filament (black circles) and HST/COS sightlines not belonging to a filament (grey circles) plotted together with the galaxies from the V8k catalogue belonging to filaments (colour-coded according to velocity).

Metal ions (Si II, Si III, Si IV, C II or C IV) were detected for 26 of the 215 Ly α filament absorbers, giving a metal detection fraction of $\sim 12\%$. Two example HST/COS spectra are shown in Fig. 3 (black) together with synthetic model spectrum (red). These example spectra give an indication of the characteristic differences in S/N in the COS data used in this study.

Figure 4, upper panel, shows the distribution of H I Ly α equivalent widths for the detected absorbers in the two sub-samples and in the combined, total sample. The lower panel instead shows the distribution of H I column densities in the filament-related absorbers, as derived from the component modelling. Both distributions mimic those seen in previous Ly α studies at $z = 0$ (Lehner et al. 2007). The sample of Danforth et al. (2016) with 2577 Ly α absorbers obtained with HST/COS shows a similar distribution with a peak in equivalent width just below 100 mÅ. The H I column-density distribution falls off below $\log N(\text{H I}) = 13.5$ due to the incompleteness in the data to detect weaker H I Ly α absorbers. Note that because of the limited spectral resolution and S/N many of the broader Ly α lines most likely are composed of individual, unresolved sub-components. The H I column-density distribution function will be discussed in Sect. 7.

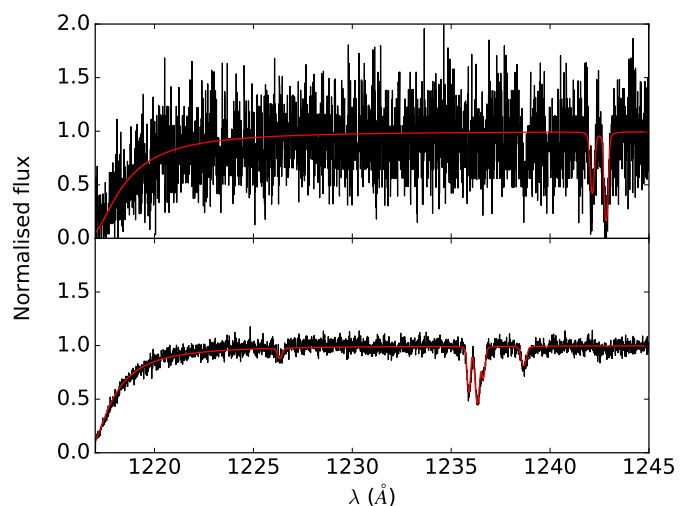


Fig. 3. HST/COS G130M spectra of the QSOs VV2006-J131545.2+152556 (upper panel) and PKS2155-304 (lower panel). The COS data are given in black, while the absorber model is plotted in red. Several Ly α absorbers are seen in these spectra. For a better visualisation, both spectra are binned over two pixels.

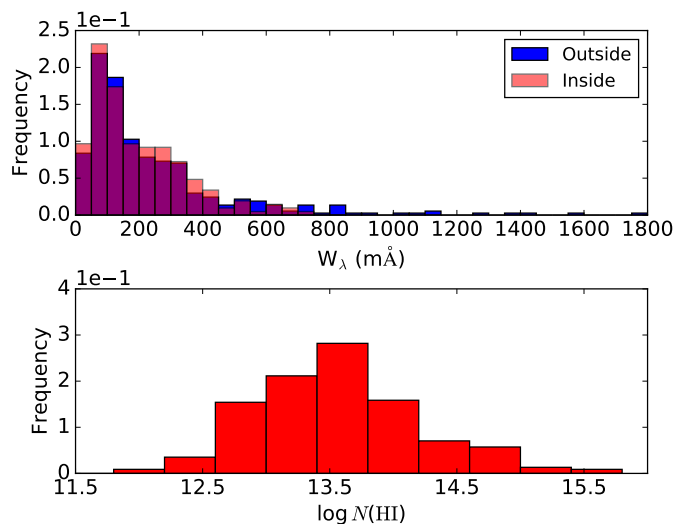


Fig. 4. Histogram of equivalent widths of Ly α absorbers (upper panel) and $\log N(\text{HI})$ in the filament-related absorbers, as derived from the component modelling (lower panel).

Errors of the measured equivalent widths have been derived with the span code (Richter et al. 2011), which takes into account the S/N around each line, the uncertainty for the local continuum placement, and possible blending effects with other lines/features. Typical 1σ errors for the equivalent widths lie around 20 mÅ. The errors in the column densities were derived based on the component-modelling method Richter et al. (2011). Here, the typical errors are on the order of ~ 0.1 dex.

The latter value is similar to the errors found by Richter et al. (2017) for the same method and a comparable COS data set. The Doppler parameters have a relatively high uncertainty, especially for higher values of b . With the majority of b -values falling between 10 and 30 km s $^{-1}$, the errors are typically ~ 5 km s $^{-1}$, with lower errors for the low end of the range of b and slightly higher errors for larger b -values. Tabulated results from our absorption-line measurements can be made available on request.

4. Characterisation of galaxy filaments

To study how the IGM is connected to its cosmological environment, it is important to characterise the geometry of the filaments, their galaxy content, and their connection to the overall large scale structure. In Fig. 5, we show the position of the galaxies in the filaments together with their radial extent in 1.5 virial radii ($1.5 R_{\text{vir}}$). Gas within this characteristic ‘sphere of influence’ can be considered as gravitationally bound to that galaxy. This plot therefore gives a first indication of how much uncovered sky there is *between* the galaxies and their spheres of influence, indicative for the projected intergalactic space in the filaments (compared to the projected circumgalactic space within $1.5 R_{\text{vir}}$). The Virgo Cluster clearly stands out, as many galaxies are overlapping in their projected spheres at $1.5 R_{\text{vir}}$, while in most other filaments, there are both regions with strong overlap and regions without overlapping halos. In Sect. 6 and in the Appendix, we will discuss also other virial radii as selection criteria.

4.1. Parametrisation of filament geometry

To define an axis for each filament, a rectangular box was generated per filament containing the galaxies therein. The dark blue filament (see Fig. 2) was split into two individual boxes because of geometrical reasons. Widths and lengths of the boxes vary for the different filaments, as they scale with the filament’s projected dimensions.

After defining the boxes sampling the individual filaments, they were each sub-divided into segments with the full width of the box and a length corresponding to 20° on the sky. Each segment overlaps with the previous one with half the area (10° length). The average longitude and latitude of the galaxies within each segment was then determined and used as an anchor point to define the filament axis. All these anchor points were connected in each filament to form its axis.

In this way, the definition of the filament axis on the sky allowed us to calculate impact parameters of the COS sightlines to the filaments. In addition, we calculated velocity gradients in the filaments, by taking the average velocity of all galaxies in each segment as velocity anchor point.

The method of using overlapping segments to determine the filament axis is similar to the approach used by Wakker et al. (2015). A difference with their approach is that they first determined which galaxies were part of the filament by looking at the velocities. We did not do this as the filaments were already defined by Courtois et al. (2013). The uncertainty on the placement of the filament axes is no more than 1.5° on the sky, less for most filaments.

The characteristics of each filament will be discussed separately in the following subsections. The orange or ‘4 clusters’ filament from Courtois et al. (2013) is not discussed here, as there are no available COS sightlines nearby.

4.2. Green filament

Perhaps the most notable of the filaments discussed here is the one containing the Virgo Cluster, located at a distance of ~ 16.5 Mpc (Mei et al. 2007) and with up to 2000 member galaxies. This filament is labelled in green in Fig. 2 and extends from the Centaurus Cluster to the Virgo Cluster in the range $l \sim 260 - 300^\circ$ and $b \sim 60 - 70^\circ$. The Virgo area has the highest galaxy density of the regions studied here.

The axis of the green filament as well as the galaxy velocities are indicated in Fig. 6a. The velocities range from ~ 3400 km s $^{-1}$ at the Centaurus Cluster to ~ -400 km s $^{-1}$. However, the velocities of the galaxies in the Virgo Cluster reach up to ~ 2500 km s $^{-1}$, indicating a large spread in velocities, just as expected for a massive galaxy cluster.

Figure 7 shows that the density along the filament varies greatly, with the Virgo Cluster being the densest region (sub-boxes 6 – 8). In total, this filament has 427 galaxies and 36 COS sightlines passing through it.

4.3. Purple filament

As mentioned in Courtois et al. (2013), the purple filament is the longest cosmological structure in space from those studied here. In projection, however, it is one of the shorter filaments on the sky. This filament was discussed in detail by Fairall et al. (1998), who named it the ‘Centaurus Wall’. A striking lack of galaxies in the regions around $b \sim 0^\circ$ is evident in Fig. 6b due to the ZOA caused by the Milky Way disk in the foreground.

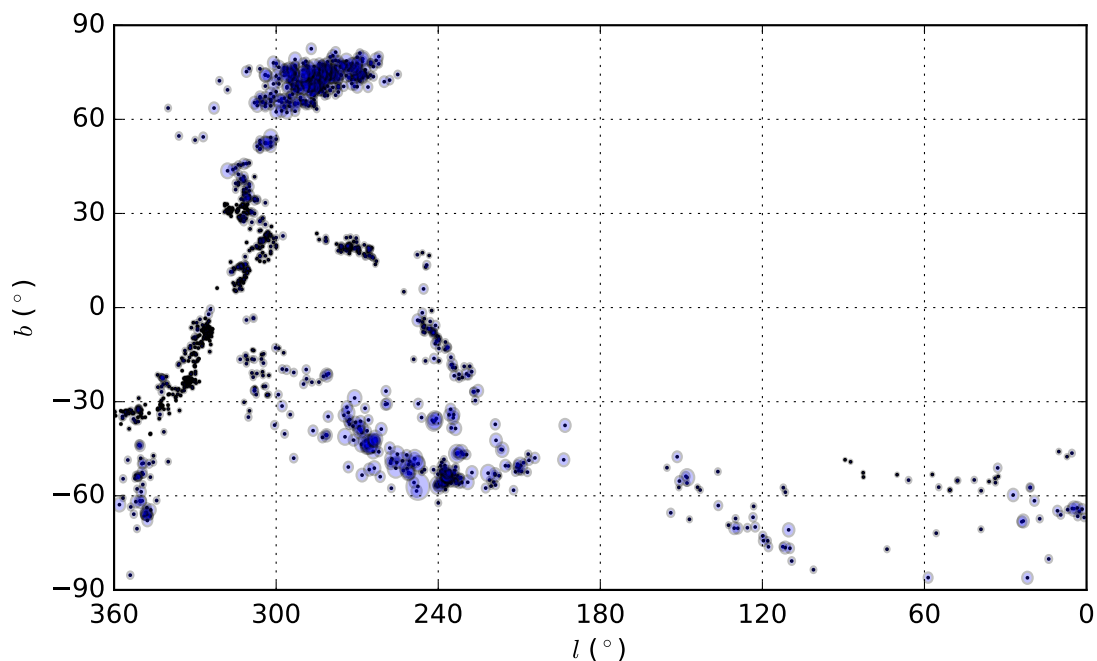


Fig. 5. Galaxies belonging to all filaments considered in this study plotted together with their projected 1.5 virial radii.

Just below this scarcely populated region is the Norma Cluster ($l \sim 325^\circ$), followed by the Pavus II Cluster ($l \sim 335^\circ$).

The purple filament contains the galaxies with the highest velocities in our sample, with v reaching up to 6500 km s^{-1} (see Fig. 6b). These high velocities indicate distances of $\leq 85 \text{ Mpc}$. It is the only filament in which the galaxy velocities strongly increase when moving away from Centaurus. As such, it extends beyond the velocity range considered in Courtois et al. (2013). Here, we consider only the part of the filament indicated by their work.

The purple filament is the densest of our defined filaments, which is not surprising as it hosts two galaxy clusters and the projection effect makes it visually compact on the sky. A total of 351 galaxies from the V8k catalogue belong to this filament, but only 2 COS sightlines, which are both shared with the dark blue filament.

4.4. Dark Blue filament

The dark blue filament represents one branch of the Southern Supercluster filament, defined in Courtois et al. (2013). Since it is clearly separated on the sky from the other branch (the cyan filament), these two branches are treated as individual filaments in this study. Starting from the Centaurus Cluster, the dark blue filament is entangled with the purple filament, but it continues to stretch out as a rather diffuse cosmological structure over the range $l \sim 0 - 180^\circ$ in the southern hemisphere. Because of the low galaxy density, the filament axis of the dark blue filament is not well defined and unsteady compared to other filaments, as can be seen in Fig. 6c. The dashed portion of the axis indicated in the figure is a result of the small number of galaxies found in this region, so the exact filament geometry in this part of the filament remains uncertain.

Figure 6 further indicates that average velocities in the dark blue filament are much lower than in the purple filament, making the two filaments easy to distinguish. The dark blue filament also exhibits two distinct velocity branches: one with veloci-

ties $\sim 2500 \text{ km s}^{-1}$ and one with $v \sim 1300 \text{ km s}^{-1}$ (see Fig. 6), further underlining the inhomogeneous morphology of this filament. This filament has only 180 galaxies and 21 COS sightlines.

4.5. Cyan filament

The second branch of the Southern Supercluster filament is indicated by the cyan colour in Fig. 2. Compared to the dark blue filament, this branch is rather densely populated and the corresponding filament axis is well defined (Fig. 6d).

As with the green and dark blue filaments, the highest velocities in the cyan filament are found near the Centaurus Cluster, with velocities decreasing as one gets closer to the Fornax Cluster. However, Fig. 6 suggests that there is a slight increase in velocity near the end of the filament at $l < 240^\circ$.

The cyan filament is made up of 289 V8k galaxies and there are 20 COS sightlines passing through it.

4.6. Magenta filament

This filament (magenta coloured in Fig. 2) contains the Antlia Cluster and also crosses the ZOA. While it is densely populated for $b > 0^\circ$ (near Centaurus), it is underdense near the ZOA and also only moderately populated at negative Galactic latitudes. This makes the transition of the filament axis from positive to negative latitudes hard to define.

As can be seen in Fig. 6e, the velocities in this filament range from 3000 km s^{-1} near the Centaurus Cluster to 1400 km s^{-1} near its end at $l = 210^\circ$ and $b = -45^\circ$. It has 143 galaxies and 2 usable COS sightlines.

5. Ly α absorption and its connection to galaxies

To learn about the relation between intervening Ly α absorption, nearby galaxies, and the local large scale structure, in which the absorbers and galaxies are embedded, we first look at the con-

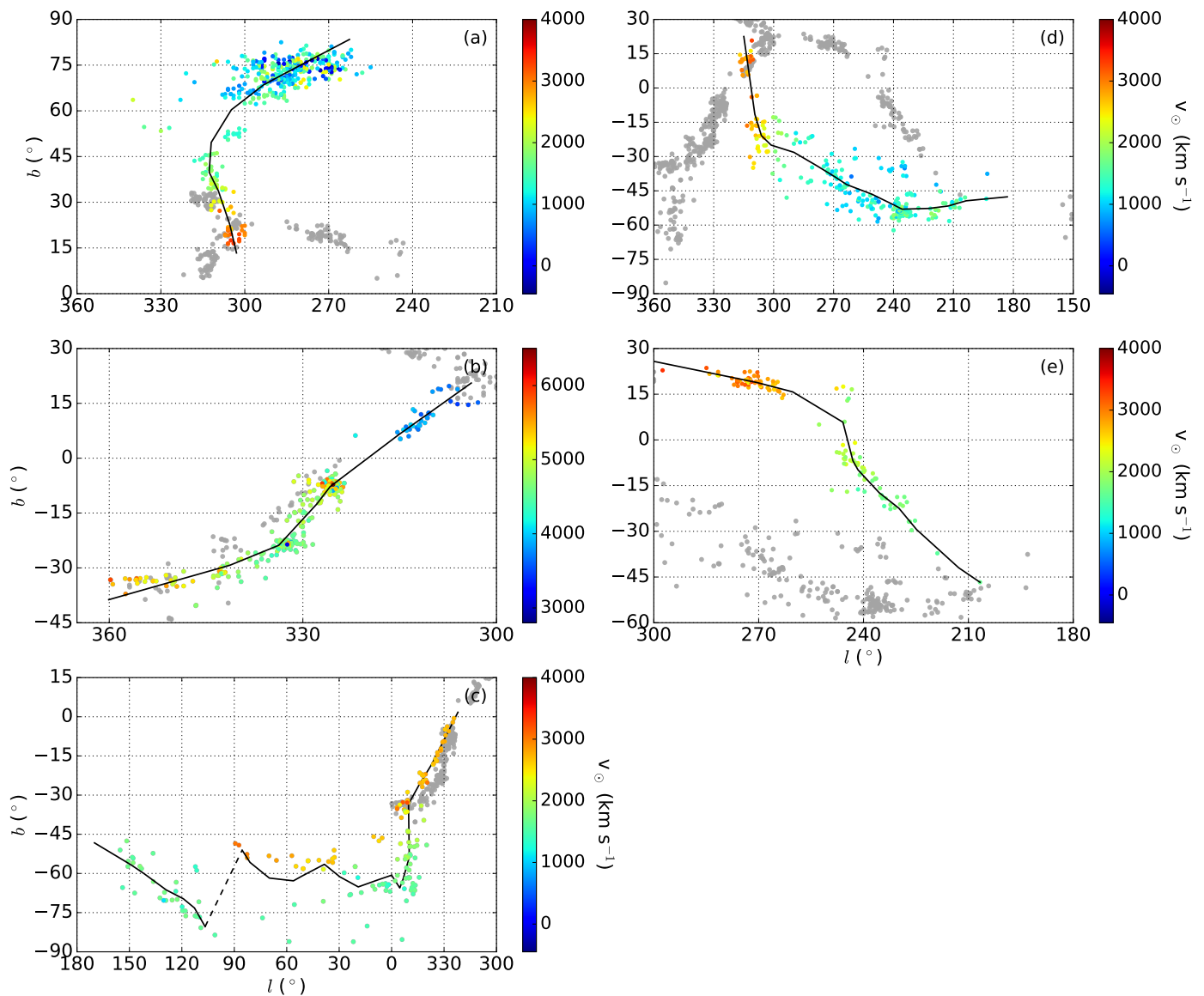


Fig. 6. Galaxies belonging to different filaments [(a): green; (b): purple; (c): dark blue; (d): cyan; (e): magenta] with their velocities colour-coded. Grey dots show galaxies belonging to one of the other filaments. The filament axes is indicated with the black solid line.

nection between Ly α absorption in the COS data and individual galaxies.

In Fig. 8, upper panel, we have plotted the equivalent widths of all Ly α absorbers against the line-of-sight impact parameter to the nearest galaxy, ρ_{gal} , that has a radial velocity within 400 km s $^{-1}$ of the absorber. For this plot, *all* V8k galaxies have been taken into account (not just the ones in filaments), as some of the absorbers might be related to galaxies outside of the main cosmological structures. We indicate absorbers that are within 1000 km s $^{-1}$ of the nearest filament in red, and those that have larger deviation velocities in blue. Non-detections have been indicated by the black crosses. The corresponding sightlines do not show any Ly α absorption in the wavelength range 1220–1243 Å.

There is an overdensity of absorbers within 1 Mpc of the nearest galaxy, many of which having equivalent widths less than $W_{\lambda} < 200$ mÅ. This overabundance of weak absorbers close to galaxies might be a selection effect. Prominent regions, such as the dense Virgo Cluster, receive more attention by researchers and are sampled by more sightlines (and by spec-

tral data with better S/N) compared to underdense cosmological regions, which typically are not as well-mapped. The highest equivalent widths of the absorbers ($W_{\lambda} > 500$ mÅ) typically are found closer to the galaxies, in line with the often observed anti-correlation between Ly α equivalent width and impact parameter (e.g. Chen et al. 2001; French & Wakker 2017). There is, however, a large scatter in this distribution, such as seen also in other studies (e.g. French & Wakker 2017). This scatter most likely is related to filament regions that have a large galaxy density and overlapping (projected) galaxy halos, such as indicated in Fig. 5. Ly α absorption that is detected along a line of sight passing through such a crowded region cannot unambiguously be related to a *particular* galaxy (such as the nearest galaxy, which is assumed here), but could be associated with the same likelihood to any other (e.g., more distant) galaxy and its extended gaseous halo that is sampled by the sightline.

The lower panel of Fig. 8 shows the Ly α equivalent width plotted against $\rho_{\text{gal}}/R_{\text{vir}}$. Again, we see the same trend for stronger absorbers to be closer to a galaxy. Out of the 208 Ly α absorption components, 29 are within 1.5 virial radii from the

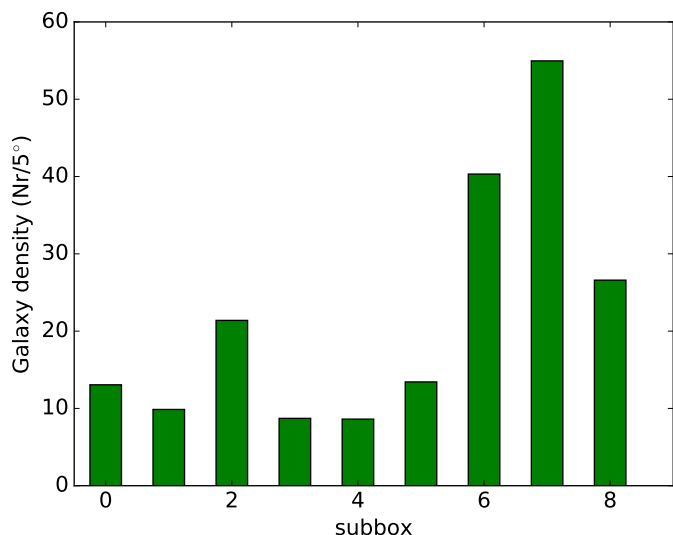


Fig. 7. Galaxy density along the green filament. The galaxy density indicates the number of galaxies within 5° on the sky for each galaxy.

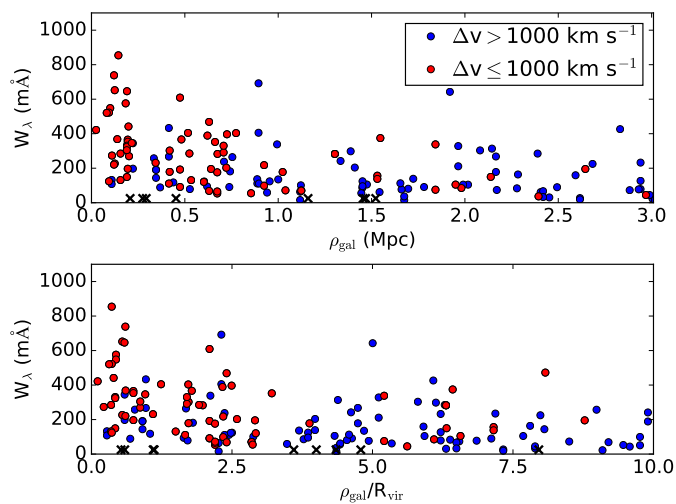


Fig. 8. Equivalent width of Ly α absorbers (blue dots) plotted against the impact parameter to the nearest galaxy (upper panel) or against the impact parameter in units of the galaxy’s virial radius (lower panel). The sample has been split into components that lie within 1000 km s^{-1} of the nearest filament segment (red) and ones with a larger velocity difference (blue). Black crosses indicate sightlines that exhibit no significant Ly α absorption in the analysed spectral region. For these, we give the distance to the nearest galaxy in the velocity range $v = 1070 - 6700 \text{ km s}^{-1}$.

nearest galaxy. Following Shull (2014); Wakker et al. (2015), this is the characteristic radius up to which the gas surrounding a galaxy is immediately associated with that galaxy and its circumgalactic gas-circulation processes (infall, outflows, mergers). It corresponds to $\sim 2 - 3$ times the gravitational radius as defined in Shull (2014). Outside of this characteristic radius, the gas is more likely associated with the superordinate cosmological environment (i.e., the group or cluster environment and the large-scale filament; but see also Sect. 6 and Fig. B.1). Wakker et al. (2015) use both this distance criterion and the criterion of absorption occurring within 400 km s^{-1} of the galaxy’s velocity to associate each absorber with either the galaxy or the filament. This velocity range (which we also adopt here; see above) is justified in view of other dynamic processes that would cause

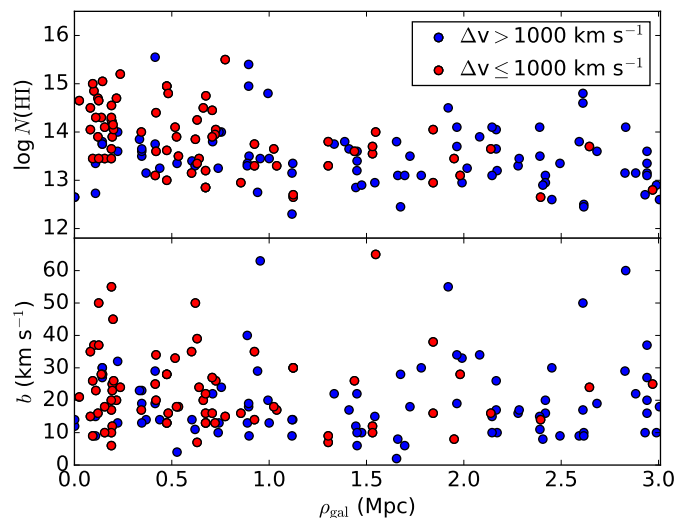


Fig. 9. Logarithmic H I column density and the Doppler parameter of Ly α absorbers are plotted against ρ_{gal} for the same two samples as shown in Fig. 8.

a Doppler shift of the gas in relation to the galaxy’s mean radial velocity, such as galaxy rotation, velocity dispersion of gas-structures within the virialised dark-matter of the host galaxy, as well as in- and outflows.

In Fig. 9 we show how the H I column density ($\log N(\text{H I})$) and the Doppler parameter (b value) vary with ρ_{gal} . Similarly to W_λ , the largest values for $\log N(\text{H I})$ and b are found at smaller impact parameters, but (again) the scatter is large.

Wakker et al. (2015) have also plotted the equivalent width versus impact parameter to the nearest galaxy for their sample. Although there are some high equivalent width absorbers at large ρ_{gal} (out to 2000 kpc), the average equivalent width decreases with increasing ρ_{gal} . Similar to our sample, Wakker et al. (2015) find the majority of the absorbers within 1 Mpc of a galaxy. Our sample, however, has a larger scatter and more strong absorbers at larger distances. Prochaska et al. (2011) also conclude there is an anti-correlation between equivalent width and galaxy impact parameter for their sample that has a maximum ρ_{gal} of 1 Mpc. In addition to stronger absorbers having lower impact parameters, their sample shows an increase of the number of weak absorbers ($W_\lambda < 100 \text{ m}\text{\AA}$) with increasing impact parameter.

6. Ly α and its connection to filaments

In Fig. 10, the filaments are plotted together with the position of the COS sightlines (filled squares) and the velocities of the detected Ly α components colour-coded (in the same way as the galaxies). Only those absorption components are considered that have velocities within 1000 km s^{-1} of the nearest filament segment. These plots are useful to visualise the large-scale kinematic trends of the absorption features along each filament, while at the same time the spatial and kinematic connection between Ly α components and individual galaxies can be explored.

In the green filament (a), Ly α absorption is predominantly found near 1500 km s^{-1} . This holds true for both the sightlines at the outskirts of the filament and those going through the Virgo Cluster. For the latter, this indicates the gas has a higher velocity than the typical velocity of galaxies in the Virgo Cluster (as mentioned earlier, the V8k catalogue takes into account the Virgo flow model by Shaya et al. (1995)). Due to the extended Ly α

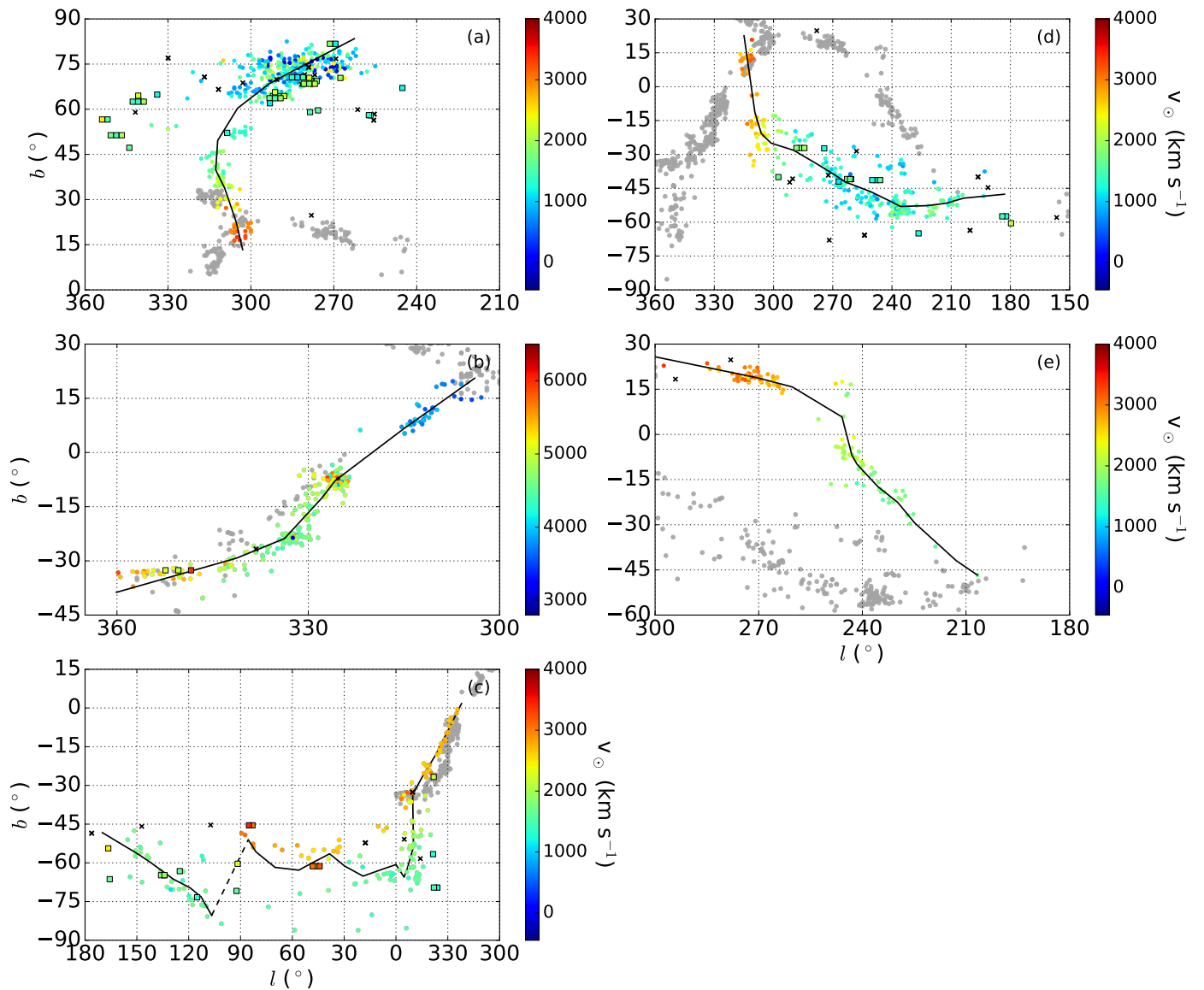


Fig. 10. Same as Fig. 6, but here with Ly α absorbers (coloured squares) overlaid that fall within 1000 km s $^{-1}$ of the filament’s velocity. Multiple absorbers along the same sightline have been given spatial offset. COS sightlines that do not exhibit Ly α absorption in this range, are indicated by black crosses.

trough of the Galactic foreground ISM absorption, intervening Ly α absorption below ~ 1100 km s $^{-1}$ cannot be measured in our COS data set, so that our absorption statistics is incomplete at the low end of the velocity distribution. Still, the trend of decreasing galaxy velocities with increasing distance to the Centaurus Cluster (see above) is not reflected in the kinematics of the detected Ly α absorbers in this filament, which appears to be independent of the large-scale galaxy kinematics.

The purple filament (b) and first section of the dark blue filament (c) overlap on the sky and have two COS sightlines in common. The different filament velocities allow us to assign the detected Ly α absorption in one of the sightlines to the purple filament, while the other sightline has one absorption component that we associate with the dark blue filament. With only 2 sightlines available for the purple filament, no clear trends can be identified.

As the dark blue filament continues, the different ‘branches’ noted earlier in Sect. 4.4 are also reflected in the velocities of the Ly α absorption components. This trend might be partly a

result of our original selecting criterion for filament-related absorbers (absorption within 1000 km s $^{-1}$ of the closest filament-segment velocity; see above). However, because of the large velocity range used, the selection criterion cannot account for the entire branching effect. Obviously, in this filament, the gas traces the velocities of the galaxies. Since this is the most diffuse filament, the chance of finding a Ly α absorber, that is not directly associated with a galaxy but rather traces the large-scale flow of matter in that filament, is higher.

The cyan filament (d) instead is well-populated with galaxies, while also being relatively long and broad. It thus has a high cross-section and there are several sightlines that pass through this structure. Also in this case, the Ly α absorption appears to follow the velocity trend of the galaxies in the filament here. Starting from Centaurus, the absorbers first exhibit velocities around 1800 km s $^{-1}$, then the velocities decrease several hundred km s $^{-1}$, to rise again slightly at the end of the filament, in line with the galaxies’ velocity pattern.

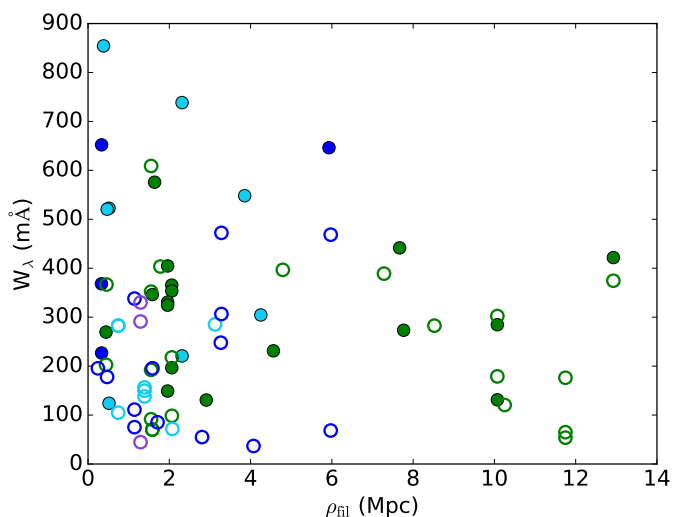


Fig. 11. Ly α equivalent width versus filament impact parameter for absorbers with velocities within 1000 km s^{-1} of the nearest filament segment. Open circles indicate absorbers that are associated with a galaxy (passing it within $1.5 R_{\text{vir}}$ and $\Delta v < 400 \text{ km s}^{-1}$), closed circles are not associated with a (known) galaxy. The different colours indicate the individual filaments.

Most of the sightlines that pass the magenta filament (e) are not suited for a spectral analysis. The one sightline that has been analysed, shows no significant absorption in the relevant velocity range, implying that no useful information is available for the magenta filament.

In analogy to Fig. 8, Fig. 11 shows the equivalent width of the Ly α absorbers, but now plotted against the *filament* impact parameter, ρ_{fil} . To evaluate whether the absorbers are related to a nearby galaxy, those absorbers that pass within $1.5 R_{\text{vir}}$ and $\Delta v < 400 \text{ km s}^{-1}$ of a galaxy are shown as open circles, whereas absorbers not associated with a (known) galaxy are indicated with closed circles. In the Appendix we show in Fig. B.1 the effect of varying the impact-parameter criterion for absorbers to be associated with a galaxy between 1.0 and $2.5 R_{\text{vir}}$ (which leads to no further insights, however).

While some of the absorbers with the highest equivalent widths are associated with a galaxy, this is not true for all strong absorbers. Neither sub-sample shows a clear, systematic trend for the equivalent width scaling with ρ_{fil} , except that the maximum Ly α equivalent width in a given ρ_{fil} bin decreases with increasing distance. However, both sub-samples show a higher absorber density within $\rho_{\text{fil}} < 3 \text{ Mpc}$ compared to more distant regions. Some of the absorbers indicated in green extend up to $\rho_{\text{fil}} = 13 \text{ Mpc}$, but these absorbers are unlikely to be part of the green filament, as the typical width of a cosmological filament is a few Mpc (Bond et al. 2010). But even if we limit our analysis to absorbers with $\rho_{\text{fil}} < 5 \text{ Mpc}$ (as in Wakker et al. 2015), the large scatter in the distribution of Ly α equivalent widths versus filament impact parameter remains.

The velocity trends for galaxies and absorbers along four filaments (green, purple, dark blue, cyan) are shown in Fig. 12. Starting point for each filament is the Centaurus-Cluster region. Here, each sub-box (segment) is defined to have a length of 10° on the sky. This is half the length of the sub-boxes (segments) used to define the filament axes (see Sect. 4.1), because here, sub-boxes (segments) do not overlap. Only for the second part of the dark blue filament (sub-boxes 12–18), a length of 20° was

chosen to have a sufficient number of galaxies available for the determination of a meaningful average velocity.

Both the green and cyan filaments (Fig. 12a and d) show a clear decrease in velocity as they extend further away from the Centaurus Cluster. For these two filaments, the velocities of the detected Ly α absorbers all lie above the lower limit of the galaxy velocity-dispersion in each sub-box, with only one exception (see sub-box 3 in the green filament, where one absorber falls just below the shaded area). This could possibly mean that there is a void of absorbers in the region between the filament and the Milky Way. However, it is important to recall that absorbers with velocities less than $\sim 1100 \text{ km s}^{-1}$ could not be measured due to the Galactic foreground absorption. This limit could also explain why there is no absorption in the lower velocity range of the Virgo Cluster (see sub-boxes 6 and 7 in Fig. 12a).

Furthermore, most absorbers in sub-boxes 2–4 and a couple in the other sub-boxes have large ρ_{fil} ($> 5 \text{ Mpc}$). The velocity spread for those absorbers in the first sub-boxes is larger and trending to slightly higher velocities than that of the galaxies. Most, however, fall within the standard deviation of the galaxy velocities.

The purple filament contains only three absorbers, all belonging to the same sightline at the end of the filament, as can be seen in Fig. 12b. The plot underlines that this filament is well-populated, with more than 50 galaxies in 4 out of 7 sub-boxes.

Just like the filament axis in Fig. 6c, the velocity trend along the dark blue filament is irregular. This trend is also reflected in the absorber velocities. While there are only a few galaxies in each sub-box, the second part of the filament contains 14 absorbers, which is comparable to the total number of absorbers in the cyan filament.

7. Absorber statistics

In quasar-absorption spectroscopy, the observed relation between the number of H I absorption systems in the column density interval ΔN (N_{HI} to $N_{\text{HI}} + dN$) and the absorption-path length interval Δx (X to $X + dX$) is commonly characterised by the differential *column density distribution function* (CDDF), $f(N_{\text{HI}})$. We use the formalism described in Lehner et al. (2007, and references therein) and adopt the following expression to describe the differential CDDF of our Ly α absorbers:

$$f(N_{\text{HI}}) dN_{\text{HI}} dX = C_{\text{HI}} N_{\text{HI}}^{-\beta} dN_{\text{HI}} dX. \quad (1)$$

Following e.g. Tytler (1987), absorption path Δx and redshift path Δz at $z \approx 0$ can be approximated by the relation

$$\Delta X = 0.5[(1 + \Delta z)^2 - 1],$$

where we calculate the redshift pathlength Δz for the various sightline samples as described in Sect. 3.2. The slope of the CDDF is given by the exponent β , while the normalisation constant, C_{HI} can be calculated via the relation

$$C_{\text{HI}} \equiv m_{\text{tot}}(1 - \beta) / \{N_{\text{max}}^{1-\beta} [1 - (N_{\text{min}}/N_{\text{max}})^{1-\beta}]\}$$

Here, m_{tot} is the total number of absorbers in the column-density interval N_{min} to N_{max} .

The column density distributions for our sample of Ly α absorbers are shown in Fig. 13. The CDDFs were fitted for Ly α components with $\log N(\text{H I}) \geq 13.2$ (maximum $\log N(\text{H I}) =$

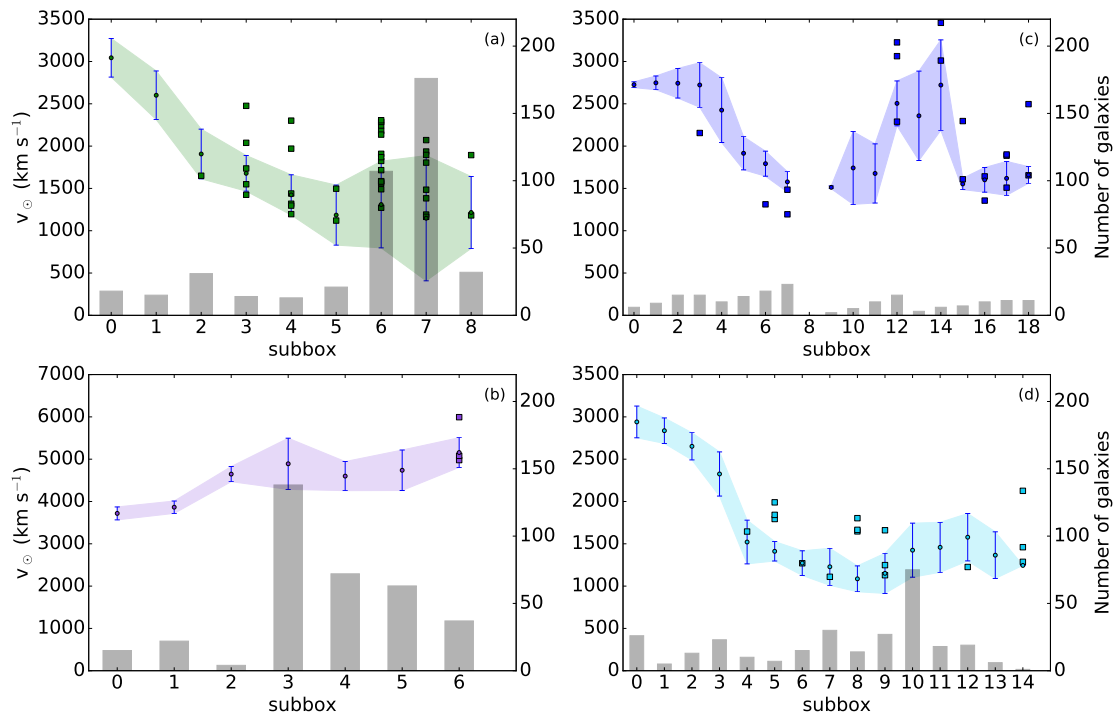


Fig. 12. Average galaxies velocities along four filaments (dots, (a): green; (b): purple; (c): dark blue; (d): cyan) plotted together with the velocities of Ly α absorbers (squares) for each sub-box (segment). The velocity dispersion is indicated by the colour-shaded area. The grey bars indicate the numbers of galaxies belonging to each sub-box (segment) in the filament.

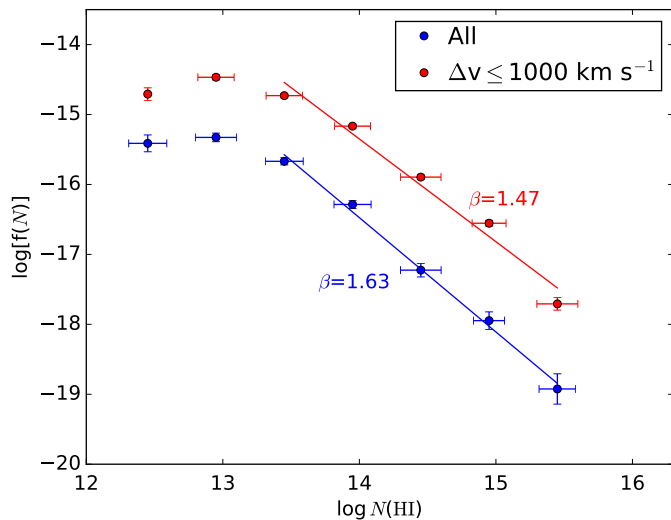


Fig. 13. H I column-density distribution function for the Ly α absorbers in sightlines close to filaments (blue) and the absorbers falling within 1000 km s $^{-1}$ from the filament velocity (red). Errors in log[f(N)] are from Poisson statistics.

15.5). For the full filament sightline sample, we derive $\beta = 1.63 \pm 0.12$, while for the sub-sample of absorbers within 1000 km s $^{-1}$ of the filament velocity we obtain $\beta = 1.47 \pm 0.24$. Using high-resolution STIS data, Lehner et al. (2007) derived $\beta = 1.76 \pm 0.06$ for their sample of narrow absorbers ($b \leq 40$ km s $^{-1}$, 110 absorbers) and $\beta = 1.84 \pm 0.06$ for $b \leq 150$ km s $^{-1}$ (140 absorbers), thus slightly steeper slopes than the distributions found here. Note that we do not split our sample based on b -values, as the fraction of absorbers with $b > 40$ km s $^{-1}$ is small ($\leq 5\%$).

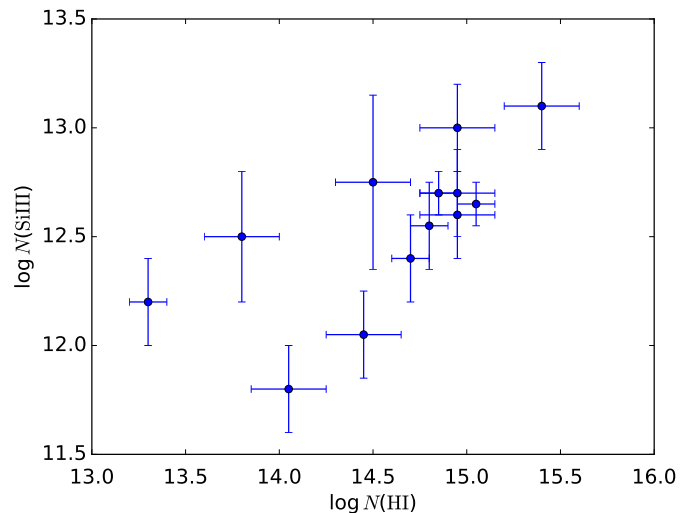


Fig. 14. Relation between log N(Si III) and log N(H I) for 13 systems in our absorber sample.

A comparison with other recent studies can be made, for example with the Danforth et al. (2016) COS study of the low-redshift IGM, which yields $\beta = 1.65 \pm 0.02$ for a redshift-limited sub-sample of 2256 absorbers. Other results are: $\beta = 1.73 \pm 0.04$ from Danforth & Shull (2008) (650 absorbers from COS), $\beta = 1.65 \pm 0.07$ by Penton et al. (2000) (187 absorbers from GHRS and STIS), and $\beta = 1.68 \pm 0.03$ by Tilton et al. (2012) (746 absorbers from STIS). Most of these values are consistent with $\beta = 1.60 - 1.70$, whereas higher values ($\beta > 1.70$) may indicate a redshift evolution of the slope between $z = 0.0 - 0.4$. Such an evolution was discussed in Danforth et al. (2016), who find a steepening of the slope with decreasing z in this redshift-range.

For our study, with $z \leq 0.0223$, the slope should be close to the value valid for the universe at $z = 0$.

Furthermore, the spectral resolution may play a role in the determination of β . For instance, the spectral resolution of COS ($R \approx 20,000$) is substantially lower than the resolution of the STIS spectrograph ($R \approx 45,000$) used by Lehner et al. (2007), so that some of our Ly α absorption components might be composed of several (unresolved) sub-components with lower column densities. The limited S/N in the COS data additionally hampers the detection of weak Ly α satellite components in the wings of stronger absorbers (see also Richter et al. 2006a, their Fig. 1).

In this series of results, the shallower CDDF ($\beta = 1.47 \pm 0.24$) for the sub-sample of velocity-selected absorbers within 1000 km s^{-1} of the filaments stands out. Although this low value is formally in agreement within its error range with the canonical value of $\beta = 1.65$, it may hint at a larger relative fraction of high-column density systems in the filaments, reflecting the spatial concentration of galaxies and the general matter overdensity in these structures. A larger sample of Ly α absorbers associated with filaments would be required to further investigate this interesting aspect on a statistically secure basis.

Like previous studies, our sample offers an opportunity to study the number of Ly α absorbers per unit redshift (dN/dz). Table 1 gives the Ly α line density for the entire sample, as well as for several subsamples. Those subsamples separate the sample into different column-density bins, allowing us to directly compare the results to the high-resolution Lehner et al. (2007) absorber sample and other studies.

For the full absorber sample (including filament and non-filament related sightlines), the Ly α line density is 116 ± 5 lines per unit redshift, but only for the filament-related subsample do we have column-density information available (see Sect. 3.2). Taking this subsample in the ranges $13.2 \leq \log N(\text{H I}) \leq 14.0$ and $13.2 \leq \log N(\text{H I}) \leq 16.5$, we derive Ly α line densities of 88 ± 8 and 98 ± 8 , respectively. These values are in good agreement with those reported by Lehner et al. (2007), who derive number densities of 80 ± 6 and 96 ± 7 for the same column-density ranges.

Our results can also be compared with those obtained from the much larger COS absorber sample presented in Danforth et al. (2016). They derive a relation for dN/dz in the form $dN(> N)/dz \approx 25(N/10^{14} \text{ cm}^{-2})^{-0.65}$. For absorbers with $\log N(\text{H I}) \geq 13.2$, this leads to $dN/dz \sim 83$, mildly lower than the values derived by us and Lehner et al. (2007), but still in fair agreement.

If we take the velocity-selected absorber sample, which potentially traces the Ly α gas associated with the filaments, we obtain a significantly higher line density of $dN/dz = 189 \pm 25$. The redshift pathlength for the velocity-selected absorber sample was calculated for each sightline by considering a velocity range of $\pm 1000 \text{ km s}^{-1}$ around the center-velocity for the filament segment that was closest to that sightline.

The value of 189 ± 25 for the velocity-selected filament sample is 93 percent higher than the value derived for the total filament-absorber sample (along the same lines of sight). This line overdensity of the Ly α forest kinematically associated with filaments obviously reflects the matter overdensity of baryons in the potential wells of these large-scale cosmological structures.

For the sake of completeness, we also show in Fig. 14 the relation between $\log N(\text{Si III})$ and $\log N(\text{H I})$ for absorbers in our sample for which both species are detected. Only for a small fraction (8.4 %) of the Ly α components, Si III can be measured, which is partly because of the velocity-shifted Si III falling in the range of Galactic Ly α absorption. Generally, $\log N(\text{Si III})$ increases with $\log N(\text{H I})$, as expected from other Si III surveys in

Table 1. Ly α line density for the full sample (filament and non-filament related sightlines), filament related sightlines, and for the velocity selected absorber sample ($\Delta v < 1000 \text{ km s}^{-1}$).

$\log N(\text{H I})$	N	dN/dz
Full sample	579	116 ± 5
Filament sample		
12.0 – 16.5	215	144 ± 11
13.2 – 14.0	132	88 ± 8
13.2 – 16.5	147	98 ± 8
Velocity-selected filament sample		
12.0 – 16.5	74	233 ± 27
13.2 – 14.0	46	145 ± 22
13.2 – 16.5	60	189 ± 25

the IGM and CGM (e.g. Richter et al. 2016), but the scatter is substantial. The small number of Si III/H I absorbers in our sample does not allow us to draw any meaningful conclusions on the metal content of the absorbers in relation to their large-scale environment.

8. Discussion on Ly α absorbers and their environment

In their study, Prochaska et al. (2011) correlated galaxies and Ly α absorbers at $z = 0.06 - 0.57$ and found that for weak absorbers ($13 \leq \log N(\text{H I}) \leq 14$) less than 20 % of the systems were associated with a known galaxy, while for strong absorbers ($\log N(\text{H I}) \geq 15$), this fraction was 80 %. The criteria they used for associating a galaxy with an absorber were the following: i) a velocity difference between absorber and galaxy of $\leq 400 \text{ km s}^{-1}$, and ii) an impact parameter of $\rho \leq 300 \text{ kpc}$. Using the same criteria, we derive for our sample that 10 % (40 %) of the low (high) column density absorbers are associated with a galaxy in the V8k galaxy sample.

Therefore, and in agreement with Prochaska et al. (2011), we find that high column density Ly α absorbers are four-times more often associated with a galaxy than low column density absorbers, but the overall fraction of absorbers for which an associated galaxy is found is only half of that in the Prochaska et al. (2011) sample. This can be attributed to the fact that the V8k catalogue is incomplete for $M_B < -16$ and $v > 1000 \text{ km s}^{-1}$, while the Prochaska et al. (2011) galaxy sample is complete up to at least $z = 0.1$ for galaxies with $L < 0.1L_*$. By comparing their observed covering fractions with a filament model, Prochaska et al. (2011) conclude that *all* Ly α absorbers are associated with either a galaxy or a filament. This view is debated by Tejos et al. (2012), however, who argue that there is an additional population of ‘random’ Ly α absorbers that reside in the underdense large-scale structure (voids).

The idea of Ly α absorbers belonging to different populations (and thus different environments) was proposed more than 25 years ago by Morris et al. (1993). By analysing Ly α absorbers in a single sightline and comparing the location of the absorbers with locations of galaxies, these authors found that the absorbers do not cluster around galaxies as strongly as galaxies cluster among themselves. On the other hand, they also found the trend that the absorbers do cluster around galaxies. From this, they concluded that there could be two populations of Ly α absorbers: one that is associated with galaxies and one that is more or less randomly distributed.

To test whether the Ly α absorbers in our sample resemble a ‘random population’, we generated two artificial populations of Ly α absorbers, both with random sky positions, random absorption velocities within the assumed $v_{\text{fil}} \pm 1000 \text{ km s}^{-1}$ velocity range of a filament, and random H I column densities weighted by the H I CDDF. For the one population, we have restricted the sample from Lehner et al. (2007) (hereafter abbreviated with L07) to the redshift range spanned by the filaments in our study and used the slope of their CDDF (resulting in 39 absorbers, $\beta = 1.76$). For the other population, we used our own absorber sample and slope (74 absorbers, $\beta = 1.47$). The normalisation constant and absorber-path length were calculated using the relations given above. All absorbers are assumed to be at a distance of $\leq 5 \text{ Mpc}$ from the nearest galaxy belonging to a filament, which was also our original criterion to select absorbers inside a filament. The fraction of the simulated absorbers in each filament was adjusted to match the real fractions found in this study. Because the dark blue and purple filaments have an overlap on the sky, their randomised simulated counterparts were generated for the both filaments combined.

Figure 15 shows a comparison of how column densities for the three different Ly α absorber samples (observed sample, random sample with own statistics, random sample with L07 statistics) depend on ρ_{gal} . Like in Sect. 5, ρ_{gal} was calculated for the nearest galaxy on the sky within a velocity interval of 400 km s^{-1} from the absorber. Clearly, the measured absorbers cluster more strongly around galaxies than both random samples. This indicates that at least some of the absorbers are associated with galaxies, as expected from previous studies (e.g. Morris & Januzzi 2006; Prochaska et al. 2011; Tejos et al. 2014; French & Wakker 2017).

A very rough estimate of the fraction of absorbers associated with a galaxy can be made by comparing the fraction of absorbers within 1.5 Mpc of a galaxy in different samples. For the measured absorbers 82 % of the absorbers have $\rho_{\text{gal}} \leq 1.5 \text{ Mpc}$, while the fraction for the randomised sample drawn from our own distribution is 53 % and for the L07 random sample it is 46 %. In conclusion, about a third of our absorbers cannot be explained by a random population and might be connected to a nearby galaxy.

When comparing the distance of the Ly α absorbers to the nearest filament axis, as shown in Fig.16, a similar, albeit less pronounced trend can be seen. Measured absorbers are generally found closer to the filament axis than a random distribution shows. One may argue that this could be a selection effect, e.g., from targeting particularly interesting areas such as the Virgo Cluster, which would result in more sightlines near the Virgo filament. However, Fig.11 showed the break-down of absorbers into different filaments, demonstrating that the absorbers belonging to the Virgo Cluster filament (green) are in fact more spread out than absorbers in other regions, speaking against such a selection effect.

To further investigate the possible clustering signal of Ly α absorbers near the filament axis, we have plotted in Figure 17 the cumulative distribution function for ρ_{fil} for the three previously mentioned absorber samples (observed sample, random sample with own statistics, random sample with L07 statistics) as well as the galaxies that constitute the filament. We also have added another absorber test sample (D16) generated from the Ly α column density distribution of absorbers reported in Danforth et al. (2016). The cumulative distribution of galaxies set the reference point, as these *define* the filament. As can be seen, the observed distribution of absorbers cluster more strongly around the filament axis than the three random absorber test distributions, but

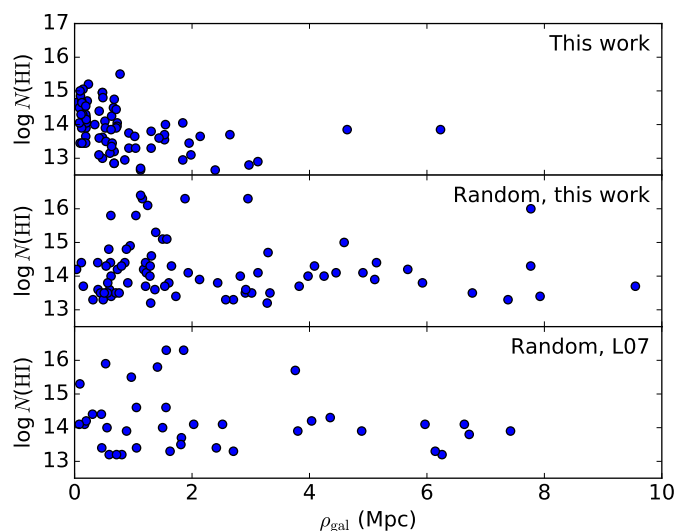


Fig. 15. H I column density versus ρ_{gal} for Ly α absorbers, i) as measured in the COS data (upper panel), ii) for a randomised sample following the CDDF in this work (middle panel), and iii) for a randomised sample following the number statistics and CDDF from Lehner et al. (2007) (lower panel).

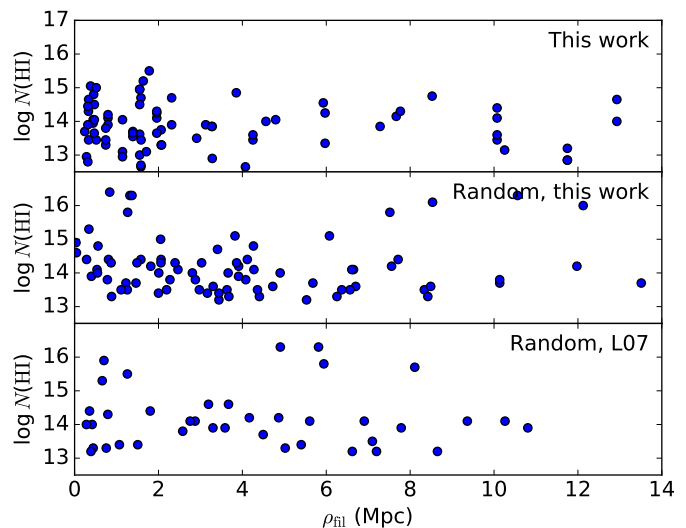


Fig. 16. Same as Fig. 15, but now for ρ_{fil} .

not as strongly as the galaxies. Within the inner 2 Mpc, in particular, the fraction of measured Ly α absorbers rises faster than the synthetic absorbers in the randomised samples.

The cumulative distribution function as shown in Fig. 17 can be compared with one for absorbers associated with galaxies. Fig. 3 in Penton et al. (2002) shows this function for 46 Ly α absorbers and subsamples thereof. Their full sample follows a distribution similar to our absorbers, with $\sim 60 \%$ found within 2 Mpc of the nearest galaxy (Penton et al. 2002) or filament (this study). Both studies show the galaxies more strongly clustered than the Ly α absorbers. Stocke et al. (2013) compared their absorber-galaxy cumulative distribution function with a random distribution concluded that absorbers are associated with galaxies in a more general way, i.e., tracing the large-scale structure instead of individual galaxies. Penton et al. (2002); Stocke et al. (2013); Keeney et al. (2018) all conclude that high-column density absorbers are more strongly correlated with galaxies than

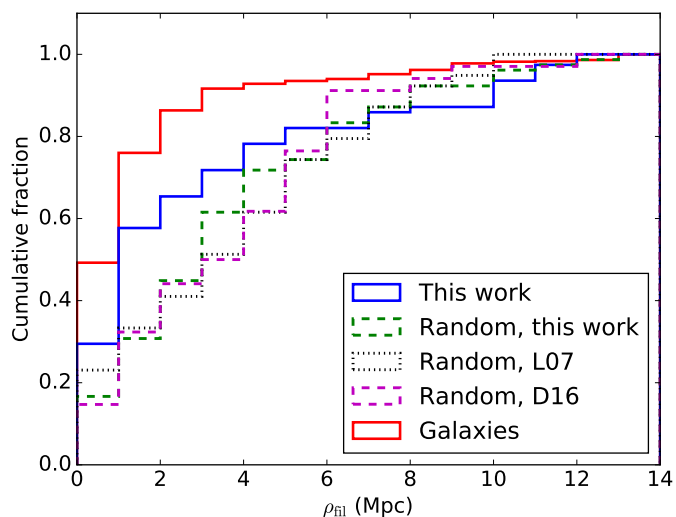


Fig. 17. Cumulative distribution function for ρ_{fil} for three different absorber samples. The measured absorbers in the COS data are indicated in blue, the random sample with own statistics is plotted in dashed green, the random sample with the L07 statistics is indicated in dotted black, and the random sample from Danforth et al. (2016) is added in dashed magenta (D16). The distribution for the galaxies is shown in red.

those with lower column densities. This is in agreement with what is found here: Ly α absorbers do not trace the same distribution as galaxies, but they are not randomly distributed around filaments either.

A Kolmogorov-Smirnov (KS) test confirms that the absorbers found in the COS data are not drawn from a random distribution. Table 2 lists the KS values and p -values for the different samples.

A KS-test can be used to compare two different samples to evaluate whether if they are drawn from the same parent distribution. A high KS value (maximum of 1) indicates a high probability that this is true. The p -value instead indicates the significance that the null hypothesis is rejected. In this case, the null hypothesis is that ρ_{fil} for the absorbers measured in this study follows the same distribution as that of a random sample, or of the galaxies in the filament. A p -value of < 0.05 means the null hypothesis can be rejected with a probability of $> 95\%$. In all three comparisons between the measurements and the random absorber samples (our own sample, randomised, and the randomised L07 and D16 samples), the KS-test indicates they do not follow the same distribution.

The low p -value that we obtain from comparing the COS absorber sample with the V8k galaxy sample in the filaments further indicates that the Ly α absorbers are not drawn from the same distribution as the galaxies. Evaluating the hypothesis that there are two populations of Ly α absorbers (e.g. Morris et al. 1993; Tejos et al. 2012), we have removed from the sample (as a test) those absorbers that we have associated with galaxies. This

Table 2. Kolmogorov-Smirnov test for impact-parameter distributions

Sample compared	KS statistics	p -value
Random, this work	0.28	0.003
Random, L07	0.31	0.011
Random, D16	0.32	0.013
V8k galaxies	0.26	0.032

has, however, no significant effect on the cumulative distribution function for ρ_{fil} .

In conclusion, the cumulative distribution functions for ρ_{fil} show that galaxies are more strongly clustered in the filaments than the Ly α absorbers that belong to the same cosmological structures. Ly α absorbers do not follow a random distribution and neither do they follow the same distribution as the galaxies that constitute large-scale filaments. There might be two (or more) separate populations of Ly α absorbers in filaments, but (from our study) there is no evidence that the Ly α absorbers that are *not* directly associated with large galaxies are randomly distributed in the field of the filament.

Deeper insights into these aspects (including other important cosmological issues such as overdensity bias-factors and how they affect the absorber/galaxy/filament statistics) are highly desirable, but will require a much larger observational data set in combination with numerical cosmological simulations.

9. Summary and concluding remarks

In this study, we have combined galaxy data of more than 30,000 nearby galaxies from the V8k catalogue Courtois et al. (2013) with HST/COS UV spectral data of 302 distant AGN to investigate the relation between intervening H I Ly α absorbers and five nearby cosmological structures (galaxy filaments) at $z \approx 0$ ($v < 6700 \text{ km s}^{-1}$).

(1) All in all, we identify 587 intervening Ly α absorbers along the 302 COS sightlines in the wavelength range between 1220 and 1243 Å. For the 91 sightlines that pass the immediate environment of the examined galaxy filaments we analysed in detail 215 (229) Ly α absorption systems (components) and derived column densities and b -values for H I (and associated metals, if available).

(2) For the individual galaxies in our sample, we have calculated the virial radii from their luminosities and the galaxy impact parameters, ρ_{gal} , to the COS sightlines. We assume 29 Ly α absorbers to be directly associated with galaxies, as they are located with 1.5 virial radii of their host galaxies and within 400 km s^{-1} of the galaxies' recession velocity.

(3) We characterise the geometry of the galaxy filament by considering the galaxy distribution in individual segments of the filaments. In this way, we define for each filament a geometrical axis that we use as reference for defining the filament impact parameters, ρ_{fil} , for those Ly α absorbers that are located within 1000 km s^{-1} of the filament.

(4) We find that the absorption velocities of the Ly α absorbers reflect the large-scale velocity pattern of the four galaxy filaments, for which sufficient absorption-line data are available. 74 absorbers are aligned in position and velocity with the galaxy filaments, indicating that these absorbers and the galaxies trace the same large-scale structure.

(5) If we relate the measured Ly α equivalent widths (or H I column densities) with the galaxy and filament impact parameters, we find that the strongest absorbers (equivalent widths $W_\lambda > 500 \text{ mÅ}$) are preferentially located in the vicinity of individual galaxies (within 3 virial radii) and/or in the vicinity of the filament axes (within 5 Mpc). The observed relations

between W and $\rho_{\text{gal}}/\rho_{\text{fil}}$ exhibit substantial scatter, however, disfavouring a simple equivalent width/impact parameter anti-correlation.

(6) We find that the measured H I components follow a column-density distribution function with a slope of $-\beta = -1.63 \pm 0.12$, a value that is typical for the low-redshift Ly α forest. Only for the sub-sample of absorbers within 1000 km s^{-1} of the filament velocity do we obtain a shallower CDDF with $\beta = 1.47 \pm 0.24$, possibly indicating an excess of high column-density absorbers in galaxy filaments when compared to the overall Ly α forest.

(7) The Ly α absorbers that lie within 1000 km s^{-1} of the nearest filament have a ~ 90 percent higher rate of incidence ($dN/dz = 189 \pm 25$ for $\log N(\text{H I}) \geq 13.2$) than the general Ly α absorber population in our sample ($dN/dz = 98 \pm 8$ for $\log N(\text{H I}) \geq 13.2$). This higher number density of Ly α absorbers per unit redshift most likely reflects the filaments' general matter overdensity.

(8) We compare the filament impact-parameter distributions of the galaxies, measured Ly α absorbers, and a (synthetic) Ly α absorber sample with randomised locations on the sky with each other. We find that the galaxies are most strongly clustered around the filament axes, while the spatial clustering of the observed Ly α absorbers around the filament axes is evident, but less pronounced. Using a KS test, we confirm that the Ly α absorbers neither follow the impact-parameter distribution of the galaxies, nor do they follow a random distribution, but represent an individual, spatially confined sample of objects.

Taken together, the results of our study underline that the relation between intervening Ly α absorbers, large-scale cosmological filaments, and individual galaxies (that constitute the filaments) in the local universe is complex and manifold, and difficult to reconstruct with existing data.

This complexity is not surprising, of course, if we recall, what Ly α absorbers actually are: they are objects that trace local gas overdensities in an extremely extended, diffuse medium that is gravitationally confined in hierarchically structured potential wells, and stirred up by large-scale matter flows and galaxy feedback. In this picture, the spatial distribution of Ly α absorbers in cosmological filaments is governed by both the distribution of individual sinks in the large-scale gravitational potential energy distribution (i.e., galaxies, galaxy groups etc.) and more (or less) stochastically distributed density fluctuations at larger scales that reflect the internal dynamics of the IGM.

For the future, we are planning to extend our study of the relation between intervening absorbers and cosmological filaments in the local universe by using a larger (and deeper) galaxy sample and additional HST/COS spectra, in combination with constrained magneto-hydrodynamic cosmological simulations of nearby cosmological structures.

Acknowledgements. The authors would like to thank the referee for his valuable comments and suggestions which helped to improve the manuscript.

References

Bond, N. A., Strauss, M. A., & Cen, R. 2010, MNRAS, 409, 156
 Bowen, D. V., Pettini, M., & Blades, J. C. 2002, ApJ, 580, 169
 Bower, R. G., Benson, A. J., Malbon, R., et al. 2006, MNRAS, 370, 645
 Cen, R. & Ostriker, J. P. 1999, ApJ, 514, 1
 Chen, H.-W., Lanzetta, K. M., Webb, J. K., & Barcons, X. 2001, ApJ, 559, 654
 Colless, M., Dalton, G., Maddox, S., et al. 2001, MNRAS, 328, 1039

Courtois, H. M., Pomarède, D., Tully, R. B., Hoffman, Y., & Courtois, D. 2013, AJ, 146, 69
 Danforth, C. W., Keeney, B. A., Tilton, E. M., et al. 2016, ApJ, 817, 111
 Danforth, C. W. & Shull, J. M. 2008, ApJ, 679, 194
 Dashtamirova, D., Fischer, W. J., et al. 2018, Cosmic Origins Spectrograph Instrument Handbook, Version 12.0 (Baltimore: STScI)
 Davé, R., Hernquist, L., Katz, N., & Weinberg, D. H. 1999, ApJ, 511, 521
 Davies, J. J., Crain, R. A., McCarthy, I. G., et al. 2019, MNRAS, 485, 3783
 Erb, D. K. 2008, ApJ, 674, 151
 Fairall, A. P., Woudt, P. A., & Kraan-Korteweg, R. C. 1998, A&AS, 127, 463
 French, D. M. & Wakker, B. P. 2017, ApJ, 837, 138
 Genzel, R., Tacconi, L. J., Gracia-Carpio, J., et al. 2010, MNRAS, 407, 2091
 Green, J. C., Froning, C. S., Osterman, S., et al. 2012, ApJ, 744, 60
 Keeney, B. A., Stocke, J. T., Pratt, C. T., et al. 2018, ApJS, 237, 11
 Lehner, N., Savage, B. D., Richter, P., et al. 2007, ApJ, 658, 680
 Madau, P., Ferrara, A., & Rees, M. J. 2001, ApJ, 555, 92
 Martizzi, D., Vogelsberger, M., Artale, M. C., et al. 2019, MNRAS, 486, 3766
 Mei, S., Blakeslee, J. P., Côté, P., et al. 2007, ApJ, 655, 144
 Morris, S. L. & Jannuzi, B. T. 2006, MNRAS, 367, 1261
 Morris, S. L., Weymann, R. J., Dressler, A., et al. 1993, ApJ, 419, 524
 Morton, D. C. 2003, ApJS, 149, 205
 Pallottini, A., Gallerani, S., & Ferrara, A. 2014, MNRAS, 444, L105
 Penton, S. V., Shull, J. M., & Stocke, J. T. 2000, ApJ, 544, 150
 Penton, S. V., Stocke, J. T., & Shull, J. M. 2002, ApJ, 565, 720
 Prochaska, J. X., Weiner, B., Chen, H. W., Mulchaey, J., & Cooksey, K. 2011, ApJ, 740, 91
 Prochaska, J. X. & Wolfe, A. M. 2009, ApJ, 696, 1543
 Richter, P., Fang, T., & Bryan, G. L. 2006a, A&A, 451, 767
 Richter, P., Fox, A. J., Wakker, B. P., et al. 2013, ApJ, 772, 111
 Richter, P., Krause, F., Fechner, C., Charlton, J. C., & Murphy, M. T. 2011, A&A, 528, A12
 Richter, P., Nuza, S. E., Fox, A. J., et al. 2017, A&A, 607, A48
 Richter, P., Paevels, F. B. S., & Kaastra, J. S. 2008, Space Sci. Rev., 134, 25
 Richter, P., Savage, B. D., Sembach, K. R., & Tripp, T. M. 2006b, A&A, 445, 827
 Richter, P., Wakker, B. P., Fechner, C., et al. 2016, A&A, 590, A68
 Saunders, W., d'Mellow, K. J., Tully, R. B., et al. 2000a, in Astronomical Society of the Pacific Conference Series, Vol. 218, Mapping the Hidden Universe: The Universe behind the Milky Way - The Universe in HI, ed. R. C. Kraan-Korteweg, P. A. Henning, & H. Andernach, 153
 Saunders, W., Sutherland, W. J., Maddox, S. J., et al. 2000b, MNRAS, 317, 55
 Shaya, E. J., Peebles, P. J. E., & Tully, R. B. 1995, ApJ, 454, 15
 Shull, J. M. 2003, in Astrophysics and Space Science Library, Vol. 281, The IGM/Galaxy Connection. The Distribution of Baryons at $z=0$, ed. J. L. Rosenberg & M. E. Putman, 1
 Shull, J. M. 2014, ApJ, 784, 142
 Shull, J. M., Smith, B. D., & Danforth, C. W. 2012, ApJ, 759, 23
 Stocke, J. T., Keeney, B. A., Danforth, C. W., et al. 2013, ApJ, 763, 148
 Tejos, N., Morris, S. L., Crighton, N. H. M., et al. 2012, MNRAS, 425, 245
 Tejos, N., Morris, S. L., Finn, C. W., et al. 2014, MNRAS, 437, 2017
 Tejos, N., Prochaska, J. X., Crighton, N. H. M., et al. 2016, MNRAS, 455, 2662
 Tilton, E. M., Danforth, C. W., Shull, J. M., & Ross, T. L. 2012, ApJ, 759, 112
 Tully, R. B., Rizzi, L., Shaya, E. J., et al. 2009, arXiv e-prints, arXiv:0902.3668
 Tumlinson, J., Shull, J. M., Rachford, B. L., et al. 2002, ApJ, 566, 857
 Tytler, D. 1987, ApJ, 321, 49
 Wakker, B. P., Hernandez, A. K., French, D. M., et al. 2015, ApJ, 814, 40
 Wakker, B. P. & Savage, B. D. 2009, ApJS, 182, 378
 York, D. G., Adelman, J., Anderson, John E., J., et al. 2000, AJ, 120, 1579

Appendix A: Signal-to-noise

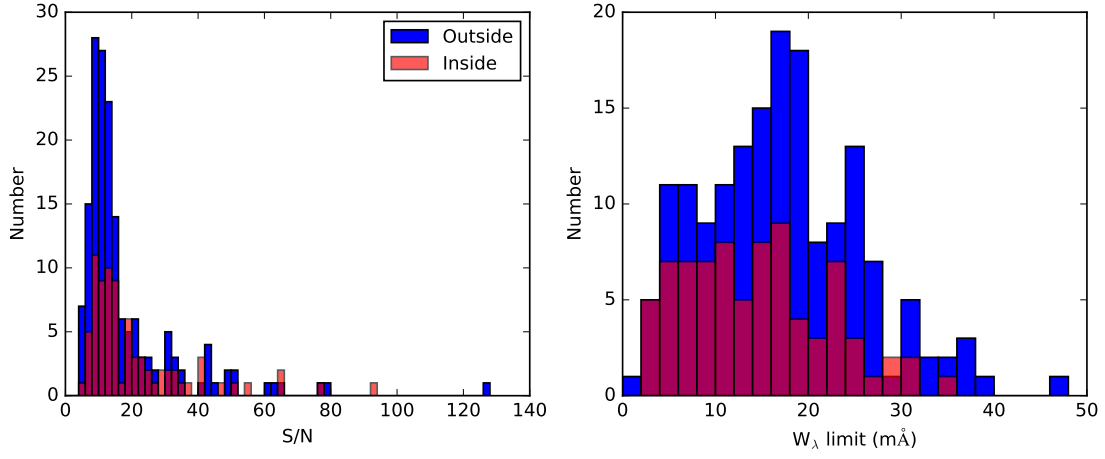


Fig. A.1. *Left panel:* distribution of the measured S/N ratios per resolution element near $\lambda 1240$ for the COS spectra that are filament-related and those outside of filaments. *Right panel:* formal 3σ detection limits for H I Ly α absorption in these spectra, based on the equation given in Tumlinson et al. (2002). Note that these values reflect the detectability of Ly α absorption as a function of the local S/N under idealised conditions (no blending, no fixed-pattern noise, perfectly known continuum flux).

Appendix B: Absorbers associated with galaxies

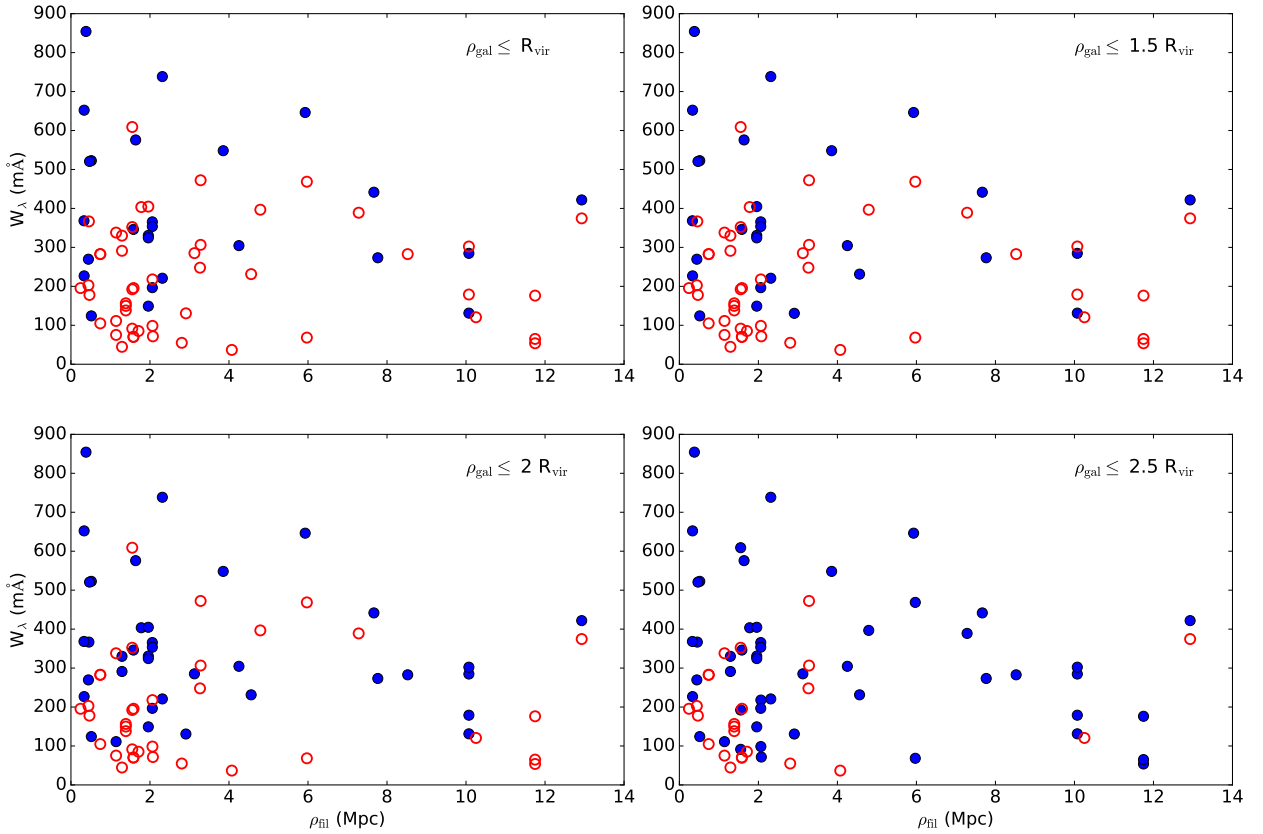


Fig. B.1. Same as Fig. 11, but now using different impact-parameter criteria ρ_{gal} for absorbers to be associated with a galaxy. Blue, filled dots are associated with a galaxy, red, open dots are not.